

Article

Selective Adsorption of Pb^{2+} in the Presence of Mg^{2+} by Layer-by-Layer Self-Assembled MnO_2 /Mxene Composite Films

Hongjing Qu ¹, Jiayan Deng ², Dan Peng ¹, Tong Wei ², Hang Zhang ² and Ruichao Peng ^{2,*} 

¹ Central-Southern Safety & Environment Technology Institute Co., Ltd., Wuhan 430051, China; whukobe@126.com (H.Q.); dfdzm@126.com (D.P.)

² College of Chemistry & Molecular Sciences, Wuhan University, Wuhan 430072, China; dengjiayan@whu.edu.cn (J.D.); 2018302030048@whu.edu.cn (T.W.); 2018302030049@whu.edu.cn (H.Z.)

* Correspondence: prc@whu.edu.cn

Abstract: A self-assembled MnO_2 /Mxene composite film was compounded with MXene nanosheets and layered crystalized MnO_2 nanosheets using surfactant sodium dodecyl sulfate (SDS) as a soft template. The obtained material was characterized by XRD, SEM, XPS, and FT-IR, which showed that the films have large surface-active functional groups and metal ion flow channels, indicating that the MnO_2 /Mxene composite films were capable of both the chemical and physical adsorption of the target heavy metal ions. The analysis of adsorption performance showed that the Pb^{2+} removal rate reached 98.3% at pH 6 and an initial Pb^{2+} concentration of 30 mg/L, while the maximum adsorption capacity could reach 1235 $\mu\text{mol/g}$. In addition, the MnO_2 /Mxene composite film had specific selectivity and recyclability. The reuse study verified that the Pb^{2+} removal rate reached 96.4% after five cycles, confirming that the MnO_2 /Mxene composite films had practical application prospects.

Keywords: MnO_2 /MXene composite film; Pb^{2+} adsorption; selective adsorption



Citation: Qu, H.; Deng, J.; Peng, D.; Wei, T.; Zhang, H.; Peng, R. Selective Adsorption of Pb^{2+} in the Presence of Mg^{2+} by Layer-by-Layer Self-Assembled MnO_2 /Mxene Composite Films. *Processes* **2022**, *10*, 641. <https://doi.org/10.3390/pr10040641>

Academic Editors: Avelino Núñez-Delgado, Zhien Zhang, Elza Bontempi, Mario Coccia, Marco Race and Yaoyu Zhou

Received: 28 February 2022

Accepted: 22 March 2022

Published: 25 March 2022

Publisher's Note: MDPI stays neutral with regard to jurisdictional claims in published maps and institutional affiliations.



Copyright: © 2022 by the authors. Licensee MDPI, Basel, Switzerland. This article is an open access article distributed under the terms and conditions of the Creative Commons Attribution (CC BY) license (<https://creativecommons.org/licenses/by/4.0/>).

1. Introduction

The presence of heavy metal ions (e.g., Pb^{2+} , As^{3+} , Cu^{2+}) in water poses a significant threat to human health through food chain transfers due to their toxicity and the tendency for bioaccumulation. Several approaches have been developed and used to remove aqueous heavy metals, such as adsorption, membrane separation, precipitation, ion exchange, photocatalysis, and electrochemical removal [1–5]. These commonly used technologies have some specific advantages as well as some inherent disadvantages. For example, precipitation is very effective and simple to operate, but the process generates a large amount of sludge, leading to secondary pollutants. Membrane separation, ion exchange, and electrochemical removal have the advantages of high efficiency and selectivity. However, they all have very high operation costs, while membrane and ion exchange also make regeneration difficult [6–8]. Of these methods, adsorption is considered one of the most efficient and effective means of removing heavy metal ions; it also has a good tolerance for a wide range of pH values and can be easily operated [9]. Currently, cheap and readily available carbon-based materials are widely used for the adsorption of heavy metal ions [10–12], but their adsorption capacity is not ideal due to the limited specific surface area. Moreover, the adsorption of heavy metal ions is not selective, so that other metal ions can easily interfere in the process owing to competitive adsorption effects.

Metal oxides, especially manganese oxide, show strong adsorption properties for metal ions due to their highly active sites. Their adsorption capacities are higher than carbon-based materials due to physical and chemical adsorption [13–15]. For example, Ma Jun et al. compounded graphene with $\delta\text{-MnO}_2$ and used it as an adsorbent to remove Pb^{2+} and Cu^{2+} from water. The maximum adsorption capacity could reach 781 $\mu\text{mol/g}$ and 1620 $\mu\text{mol/g}$, respectively, where Pb^{2+} and Cu^{2+} could be adsorbed on the surface of the composite and enter the inter-layers of MnO_2 to cause adsorption [12]. Eun-Ju Kim et al. synthesized a

three-dimensional MnO₂ loaded with magnetic Fe₃O₄ by a hydrothermal method, and its maximum adsorption capacity for Cd is 53.2 mg/g. In addition, the adsorption rate for different metal ions follow the order Cu(II) > Pb(II) > Cd(II) > Zn(II) [16]. However, the following problems exist when using manganese oxide as an adsorbent for heavy metal ions, making it a challenge to meet the needs of practical applications. First, the adsorption effect of manganese oxide is often disturbed by other cations in the solution, and the selective adsorption characteristics are not prominent. Second, manganese oxide has good dispersibility, which facilitates adsorption but makes recycling difficult.

MXene is a carbon-based compound with a two-dimensional crystal structure obtained by etching an intermediate metal layer from the MAX phase material. Due to its typical layered structure and rich surface characteristics, MXene shows excellent adsorption properties for heavy metal ions and organic pollutants [17–21]. Unlike other carbon-based adsorbents, MXene can selectively adsorb metal ions from water. For instance, the selective adsorption properties of two-dimensional titanium carbide on Pb²⁺ were investigated by Tian Yongjun et al. Their results showed that the hydroxyl functional group on the surface of titanium carbide gives it excellent selective adsorption properties for Pb²⁺, even if high concentrations of Mg²⁺ or Ca²⁺ cations existing in the solution [22].

In this paper, a wet-chemistry method was used to synthesize monolayer manganese oxide nanosheets under the induction of surfactants. Moreover, MXene, which is currently on the cutting edge of material science research, was applied to modify and functionalize the MnO₂ nanosheet to tackle the difficulties mentioned above and improve the selectivity and regeneration ability of the adsorbent. Therefore, monolayer MnO₂ nanosheets were self-assembled layer by layer with MXene nanosheets to form a self-supporting MnO₂/MXene composite film and then used for the selective adsorption of Pb²⁺. The adsorption characteristics of the MnO₂/MXene composite film were systematically investigated with various experimental parameters, such as solution pH value, adsorption time, and initial metal ion concentration. Meanwhile, the removal rate of Pb²⁺ over five cycles and the effects of other metal cations on the adsorption properties of Pb²⁺ were also investigated. The results proved that the MnO₂/MXene composite film has a high adsorption capacity and some degree of adsorption selectivity and stability for Pb²⁺. It also has the advantages of being easy to recycle and reuse.

2. Materials and Methods

2.1. Synthesis of Monolayer Manganese Oxide Nanosheets

Three grams of SDS powder was dissolved in 100 mL of deionized water, magnetically stirred well; then, 1.5 mL of H₂SO₄ was added and stirred to obtain a clear and transparent solution. Afterward, the solution was heated and stirred in an oil bath at 90 °C for 15 min and 0.8 g of KMnO₄ powder was added, and the reaction was performed at that temperature for 1 h. Finally, the mixture was cooled and washed with deionized water to remove excess surfactant and freeze-dried to obtain the monolayer MnO₂ nanosheets [23].

2.2. Preparation of MnO₂/MXene Composite Films

Ten milligrams of the above single-layer MnO₂ nanosheets were weighed and dispersed in 100 mL of deionized water; then, 2 mg of commercially available MXene solution was added, and after ultrasonic dispersion for 30 min, vacuum filtration was performed to obtain a MnO₂/MXene composite self-supporting film [24].

2.3. Characterization Test

Field emission scanning electron microscope (SEM, Zeiss SIGMA, Carl Zeiss AG, Jena, Germany), and transmission electron microscope (TEM, JEM-2100, JEOL, Tokyo, Japan) were applied for the morphological characterization of the MnO₂/MXene composite film, while the X-ray diffraction patterns were recorded on the X-ray diffractometer (XRD, XPert Pro, PANalytical Corporation, Malvern, UK) and fully automatic rapid comparison on the Surface area and porosity analyzer (BET, ASAP 2020, McMerritik (Shanghai) In-

strument Co., Ltd., Shanghai, China) The photoelectron spectra were recorded on X-ray photoelectron spectrometer (XPS, ESCALAB 250Xi, Thermo Fisher, Waltham, MA, USA), continuous light source atomic absorption spectrometer (contrAA700, Analytik Jena AG, Thuringia, Germany), while the IR spectra were recorded on a Thermo FT-IR 5700 IR spectrometer (KBr).

2.4. Heavy Metal Ion Adsorption Test

To start, 30 mg/L Pb^{2+} solution was taken as the target heavy metal ion solution, and 12 mg of $\text{MnO}_2/\text{MXene}$ composite film was weighed and placed in 100 mL of Pb^{2+} -containing solution as the pH value was adjusted from 3 to 7, and adsorption equilibrium was reached by stirring at a low speed at room temperature. Atomic absorption spectrometry was used to measure the changes in the concentration of heavy metal ions (Pb^{2+}) in different pH environments and at different adsorption times, and the adsorption capacity and removal rate were calculated. In addition, the adsorption characteristics of $\text{MnO}_2/\text{MXene}$ composite films were also investigated when the solution pH was 6 and the initial concentration of Pb^{2+} was from 10 to 90 mg/L to evaluate the influence of different initial concentrations on the adsorption efficiency of the films.

Adsorption capacity was calculated by using the mass balance equation for the adsorption (1):

$$q = \frac{(C_0 - C_e) \times V}{m} \quad (1)$$

In addition, the *removal rate* (%) was calculated from the Equation (2):

$$\text{Removal rate}(\%) = \frac{(C_0 - C_e) \times 100\%}{C_0} \quad (2)$$

where q is the adsorption capacity (mg/g) at equilibrium, C_0 and C_e are the initial and the equilibrium concentrations (mg/L), respectively, V is the volume (L) of the solution, and m is the mass (g) of the adsorbent used [25].

3. Results

3.1. Morphology and Structure Characterization

Figure 1A–C shows the cross-sectional and surface SEM images of the commercially available MXene solution after filtration. As MXene has a typical two-dimensional nanosheet structure, a layer-by-layer self-assembled film can be formed by suction filtration. What can be seen from Figure 1C is that the surface of MXene still maintains a good nanosheet morphology after suction filtration. Figure 1D–E shows the cross-sectional SEM images of the $\text{MnO}_2/\text{MXene}$ composite films, with the self-assembled films obtained by filtration after the addition of MnO_2 nanosheets. In comparison with the cross-sectional figures of the MXene films, it can be seen that the stacking of nanosheets in the $\text{MnO}_2/\text{MXene}$ composite films is more fluffy; this provides more adsorption sites than the dense MXene films and is more conducive to the flow and adsorption of metal ions between the nanosheet layers. In addition, the cross-sectional surface sweep result of the $\text{MnO}_2/\text{MXene}$ composite films shows that all the elements can be uniformly distributed in the composite films (as shown in Figure 1F), indicating that MnO_2 and MXene are alternately stacked. In addition, Ti and C were derived from MXene (TiC), Mn and O originated from MnO_2 nanosheets, while K was introduced by the MnO_2 preparation process and was present between the lattice layers of MnO_2 , supporting its layered crystal structure and maintaining charge balance.

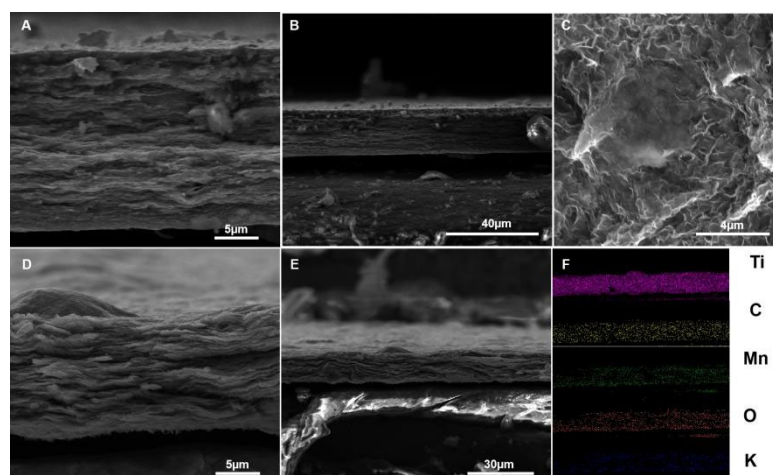


Figure 1. (A–C) SEM images of the cross-section and surface of the commercially available MXene solution after suction filtration. (D,E) SEM images of the cross-section of the MnO₂/MXene composite film. (F) Element distribution in the MnO₂/MXene composite film.

Figure 2 shows the XRD pattern of the MnO₂/MXene composite film. The peaks at 5.6° and 27.1° are characteristic of 2D Ti₃C₂, where 5.6° corresponds to the crystal plane (002), indicating a layer spacing of 1.56 nm for Ti₃C₂. Similarly, 17.1°, 29.2°, and 36.3° correspond to the characteristic peaks of 2D MnO₂. No characteristic peaks of other heterogeneous phases were observed, indicating that the prepared material was the pure-phase MnO₂/MXene composite.

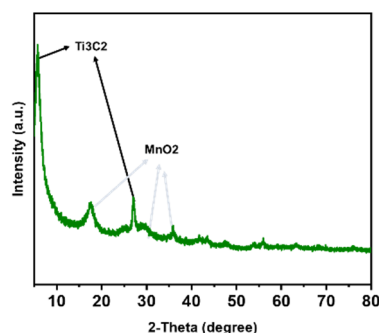


Figure 2. XRD patterns of MnO₂/MXene composite films.

Furthermore, the XPS of the MXene, MnO₂, and MnO₂/MXene composite films were tested to characterize their surface or near-surface valence information. For MXene (Figure 3), it is evident from the XPS pattern that it contains a certain amount of O and F in addition to the elements Ti and C. More specifically, for Ti2p, the characteristic peaks consist of Ti-O-Ti, Ti-OH, and Ti-C, while those of C1s are derived from C impurities introduced during the testing process in addition to Ti-C and C-OH, and the characteristic peaks of O1s consist of Ti-O-Ti, Ti-OH, and C-OH. The above test results indicate that the surface of MXene contains a large amount of surface functional groups, such as C-OH, Ti-OH, and F⁻, which are all capable of bonding heavy metal ions in water to achieve efficient adsorption. The surface valence properties of the prepared MnO₂ nanosheets were characterized by XPS, as shown in Figure 4, where the characteristic peak of Mn2p indicates that the surface is composed of Mn³⁺ and Mn⁴⁺. The presence of Mn³⁺ makes the surface of MnO₂ negatively charged and causes oxygen defects, which is beneficial for the adsorption of positively charged metal cations in solution to achieve charge balance. The O1s characteristic peak, on the other hand, consists of Mn-O-Mn, Mn-OH, and the adsorbed water on the surface. As shown in Figure 5, after compounding, the MnO₂/MXene composite film results in the

characteristic peaks of both MXene and MnO_2 . Therefore, it has the surface properties of both MXene and MnO_2 .

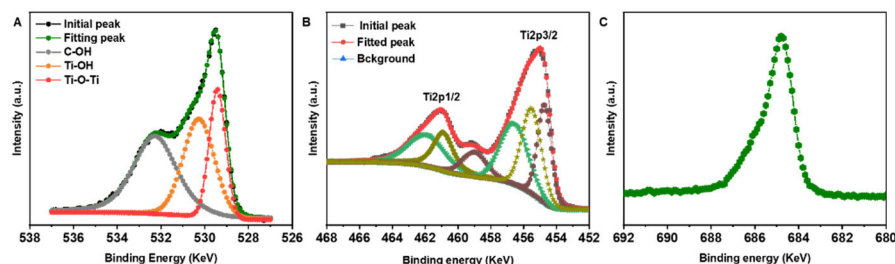


Figure 3. XPS spectra of MXene: (A) is O1s, (B) is Ti2p, and (C) is F1s.

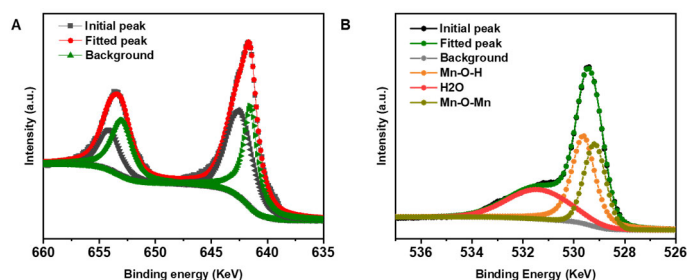


Figure 4. XPS spectrum of MnO_2 : (A) is Mn2p and (B) is O1s.

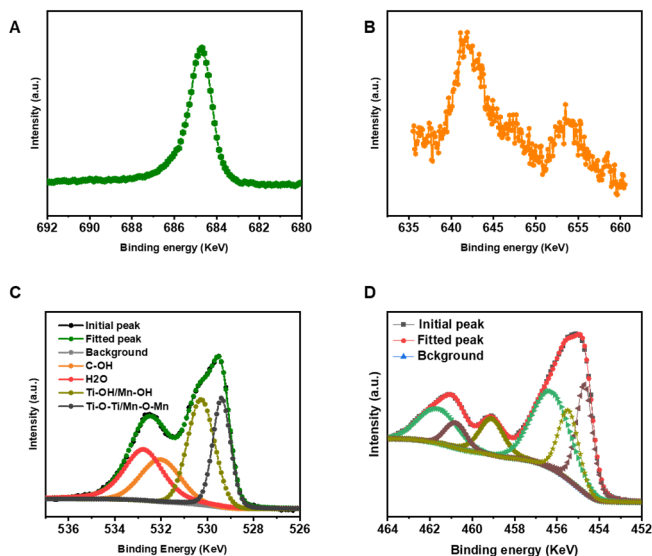


Figure 5. XPS spectrum of $\text{MnO}_2/\text{MXene}$ composite films: (A) is F1s, (B) is Mn2p, (C) is O1s, and (D) is Ti2p.

As shown in the FT-IR spectrum (Figure 6), the wide bands at 1640 and 3292 cm^{-1} in the $\text{MnO}_2/\text{MXene}$ composite film represents the bending vibration of water molecules and the O-H contraction vibration of water molecules, respectively, while the characteristic peaks of Mn-O and Ti-C are found between 600 and 700 cm^{-1} [26].

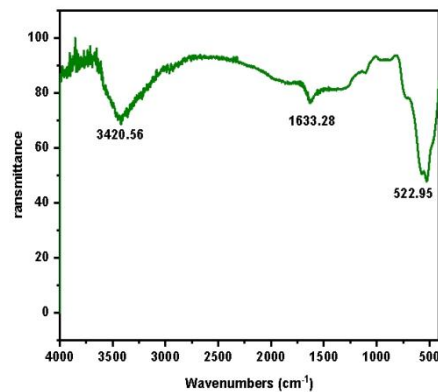


Figure 6. FT-IR spectrum of MnO₂/MXene composite films.

3.2. Study of Adsorption Performance

The above characterizations show that the synthesis of MnO₂ nanosheets using surfactants as soft templates and their composites with MXene nanosheets can self-assemble into thin films, which combines the surface properties of MnO₂ and MXene with abundant surface active sites. In addition, both MnO₂ and MXene are typical two-dimensional crystalline structures with large layer spacing; indeed, the layer spacing of MXene can reach 1.56 nm, which provides more adsorption channels for metal ion adsorption. Moreover, the microscopic morphology of the stacked layers can also provide adsorption channels for metal ions (Figure 7).

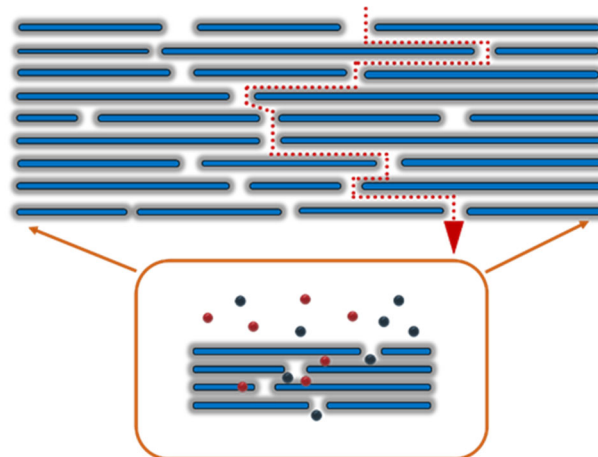


Figure 7. Schematic diagram of adsorption of heavy metal ions by MnO₂/MXene composite film [27].

3.2.1. Effect of pH on Adsorption Performance

Figure 8 shows the adsorption characteristics of the MnO₂/MXene composite film at different pH values. It can be seen that the MnO₂/MXene composite film can be used in a wide range of pH solutions, and that the removal rate of Pb²⁺ increases as the pH value rises. The removal rate was 28.3% when the pH was 3 and leveled off at pH 6 (reaching 98.3%), indicating that the pH of the solution has a significant effect on the adsorption of Pb²⁺. As the surface of the MnO₂/MXene composite film has abundant -OH groups, the negative charge on its surface increases as the pH value increases. Therefore, at low pH values, the adsorption of Pb²⁺ is low and gradually increases with the increase in pH value as H⁺ in solution competes for the adsorption of -OH on the surface of the MnO₂/MXene composite film.

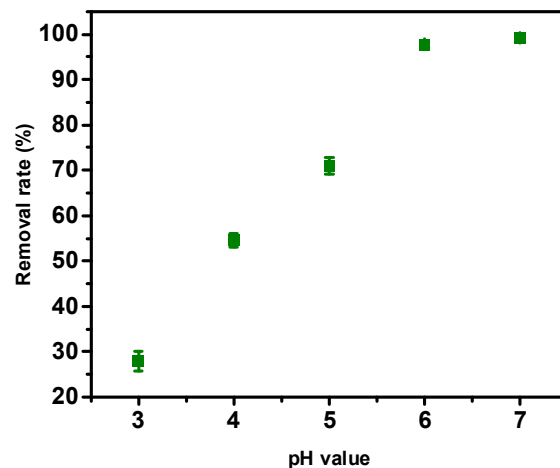


Figure 8. Removal rate of Pb^{2+} under different pH values. (Experimental conditions: $MnO_2/Mxene$ composite films 12 mg, solution volume 100 mL $C_{Pb^{2+}} = 30$ mg/L, 25 °C).

3.2.2. Effect of Adsorption Time on Adsorption Performance

The adsorption kinetics experiments of $MnO_2/MXene$ composite films were investigated when the solution pH was 6 (Figure 9). The removal of Pb^{2+} was only 27.4% within the initial hour. However, the removal increased to 98.3% after 8 h of reaction and reached adsorption equilibrium. Compared to other conventional powder adsorbents, the $MnO_2/MXene$ composite film took longer to reach adsorption saturation due to the lower specific surface area of the $MnO_2/MXene$ composite film, which exposed a smaller amount of metal ions in a short period. However, over time, heavy metal ions were able to flow in the inter-layer channels of the $MnO_2/MXene$ composite film and achieve the adsorption of metal ions. Therefore, although the time to achieve adsorption equilibrium was prolonged, the $MnO_2/MXene$ composite film still had a high Pb^{2+} removal rate. Furthermore, the longer adsorption equilibrium time also indicated that the chemical adsorption mechanism plays a decisive role in the adsorption rate of the reaction during the adsorption of Pb^{2+} by the $MnO_2/Mxene$ composite film.

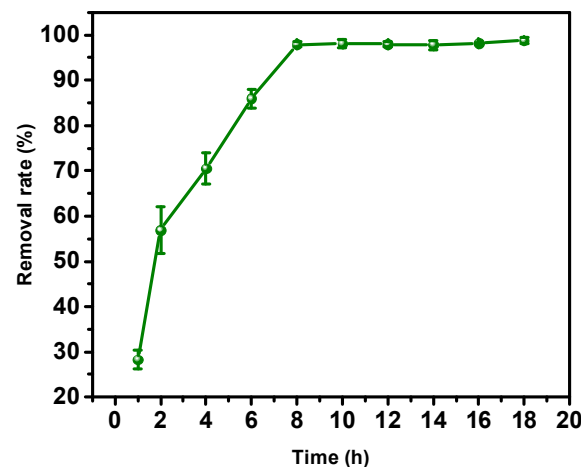


Figure 9. The removal rate of Pb^{2+} at different adsorption times. (Experimental conditions: pH = 6, $MnO_2/Mxene$ composite films 12 mg, solution volume 100 mL, $C_{Pb^{2+}} = 30$ mg/L, 25 °C).

3.2.3. Effect of Initial Concentration on the Adsorption Capacity

Figure 10 explores the effect of the initial concentration on the adsorption capacity when the pH is 6. The $MnO_2/MXene$ composite film adsorption capacity was 401.4 $\mu\text{mol/g}$ when the initial concentration of Pb^{2+} was 10 mg/L and reached 1187 $\mu\text{mol/g}$ at 30 mg/L and 1235 $\mu\text{mol/g}$ at 90 mg/L. As the initial concentration of Pb^{2+} continued to increase,

the adsorption capacity did not increase significantly. The excellent adsorption properties of MnO₂/MXene composite films can be attributed to two factors. First, the -OH, F⁻ and defects on the surface of the MnO₂/MXene composite film can act as ligands for metal ions, thus achieving chemical complex adsorption. Second, the MnO₂/MXene composite film has a layered crystal structure, and its layer spacing and two-dimensional channels formed by layer stacking further provide adsorption sites.

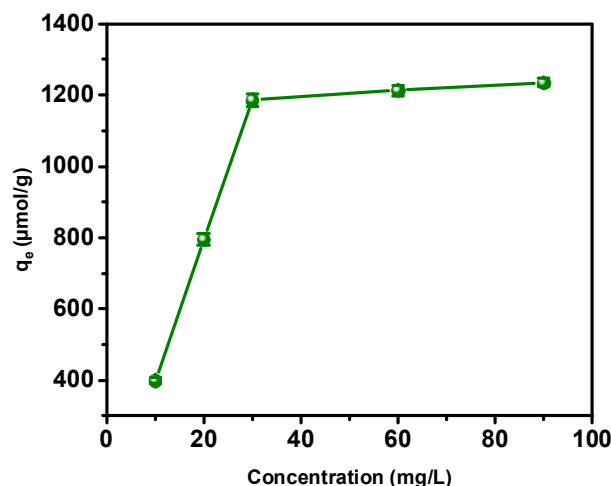


Figure 10. The adsorption capacity of Pb²⁺ under different initial concentrations. (Experimental conditions: pH = 6, MnO₂/MXene composite films 12 mg, solution volume 100 mL, 25 °C).

3.2.4. Cycling Performance Test of MnO₂/MXene Composite Film

In addition, MnO₂/MXene composite films can easily be recycled after use for heavy metal ion adsorption. Compared with traditional powder adsorbents, film-based adsorbents do not possess advantages in terms of adsorption time, but can be easily recycled without causing secondary contamination of water bodies. After the adsorption test, the MnO₂/MXene composite film was regenerated to verify its recycling characteristics. As shown in Figure 11, the Pb²⁺ removal rate remained at 96.4% after five cycles, and the adsorption performance was only 1.9% lower than the first adsorption, demonstrating the excellent stability of the material to cycling.

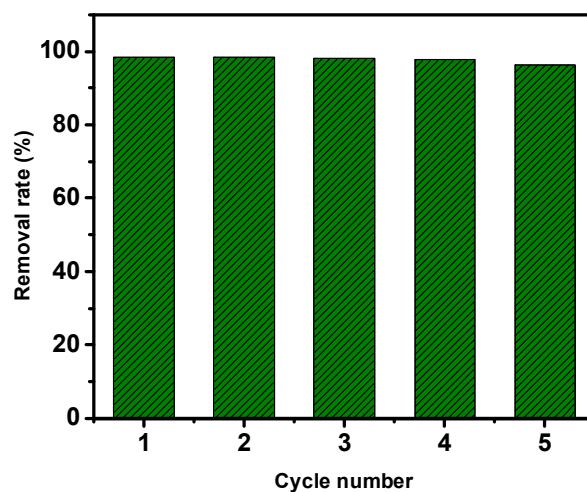


Figure 11. The removal rate of Pb²⁺ during cycling. (Experimental conditions: pH = 6, MnO₂/MXene composite films 12 mg, solution volume 100 mL $C_{Pb^{2+}} = 30$ mg/L, 25 °C).

3.2.5. The Effect of Other Metal Cations on the Adsorption Performance

Actual industrial wastewater contains large amounts of heavy metal ions and other metal cations, such as Mg^{2+} , Ca^{2+} , and K^+ . These unavoidable cations can interfere with the adsorption of Pb^{2+} and affect the adsorption capacity. In order to explore the effect of other metal cations on the adsorption performance of Pb^{2+} by MnO_2 /Mxene composite films, a mixed solution containing both Mg^{2+} and Pb^{2+} was served as the target solution to determine the adsorption characteristics at different Mg^{2+} contents. The concentration of Pb^{2+} in the fixed mixed solution was 30 mg/L. As shown in Figure 12, the Pb^{2+} removal rate decreased as the concentration of Mg^{2+} increased in the mixed solution. Although the Mg^{2+} content was much larger than that of Pb^{2+} , showing that the MnO_2 /Mxene composite film still had excellent adsorption characteristics for Pb^{2+} . For example, when the concentration ratio of Mg^{2+}/Pb^{2+} was 10:1, the removal rate of Pb^{2+} could still reach 61.7%. This result indicated that although there was a certain degree of competition of Mg^{2+} on the adsorption of Pb^{2+} , the MnO_2 /MXene composite film retains a selectivity for the adsorption of Pb^{2+} , proving its promising prospects for practical wastewater treatment applications.

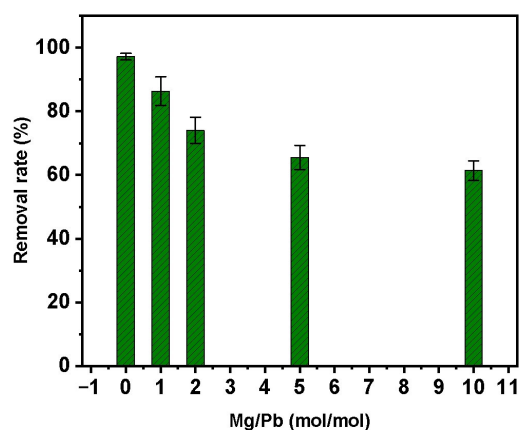


Figure 12. Pb^{2+} removal rate at different concentrations of Mg^{2+} . (Experimental conditions: pH = 6, MnO_2 /Mxene composite films 12 mg, solution volume 100 mL, $C_{Pb^{2+}} = 30$ mg/L, 25 °C).

3.2.6. Adsorption Kinetic of MnO_2 /Mxene Composite Films

The modeling of adsorption kinetics was conducted by using pseudo-second-order models with linear fitting (Figure 13):

$$\frac{t}{q_t} = \frac{1}{k q_e^2} + \frac{1}{q_e} t \quad (3)$$

where k is the pseudo-second-order adsorption rate constant ($g \cdot mmol^{-1} \cdot min^{-1}$); t is the adsorption time, q_e and q_t are the adsorption rate ($mmol \cdot g^{-1}$) at equilibrium and at time t , respectively.

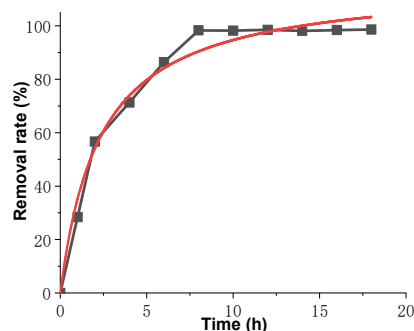


Figure 13. Pseudo-second-order models with linear fitting.

According to the Table 1 and Figure 13, the mechanism of the adsorption contains both physical adsorption and chemical adsorption, and the long adsorption equilibrium time also indicates that the MnO₂/MXene composite film on Pb²⁺ is the chemical adsorption mechanism plays a decisive role in the adsorption rate of the reaction.

Table 1. Kinetic parameters for the pseudo-second-order models for the adsorption.

q _e	k	R ²
116.53	0.433	0.98462

3.2.7. Comparison of Various MnO₂-Based Adsorbents for Pb(II)

The comparison of the maximum adsorption capacities of the obtained MnO₂/MXene composite films and various MnO₂-based adsorbents for Pb²⁺ is listed in Table 2, which shows that the MnO₂/MXene composite films might be an ideal adsorbent for aqueous Pb(II).

Table 2. Comparison of the maximum adsorption capacities of various MnO₂-based adsorbents for Pb(II).

Adsorbent	Adsorption Capacity (mg/g)	Reference
ε-MnO ₂ nanoflowers	239.7	[28]
g-C ₃ N ₄ /MnO ₂ composite	204	[29]
α-MnO ₂	124.87	[25]
MnO ₂ modified magnetic graphitic carbon nitride composite	187.6	[30]
graphene nanosheet/δ-MnO ₂	781 μmol/g (161.6 mg/g)	[27]
MnO ₂ /MXene composite films	1235 μmol/g (255.6 mg/g)	This work

4. Conclusions

In this paper, the MnO₂/Mxene composite films were prepared by a layer-by-layer self-assembly process using SDS as a soft template and applied to the adsorption of Pb²⁺ in water. The effects of solution pH, adsorption time, initial concentration, and impurity ions on the adsorption of Pb²⁺ were investigated.

- (1) The pH value of the solution, adsorption time, and initial concentration all significantly affect the adsorption of Pb²⁺. The removal of Pb²⁺ by the MnO₂/Mxene composite film reached 98.3% at pH 6 and reached adsorption equilibrium at 8 h. Increasing the content of Pb²⁺ in the initial solution can enhance the adsorption capacity of the MnO₂/Mxene composite film, which reached 1235 μmol/g when the initial concentration of Pb²⁺ was 90 mg/L.
- (2) The MnO₂/MXene composite film has a particular selectivity for Pb²⁺ adsorption, and the removal rate of Pb²⁺ can still reach 61.7% in the solution with high Mg²⁺ content (Mg²⁺/Pb²⁺ = 10:1).
- (3) The MnO₂/Mxene composite film has the property of easy recovery; after five cycles of testing, its Pb²⁺ removal rate can still reach 96.4%.
- (4) The process of Pb²⁺ adsorption of by the MnO₂/Mxene composite film is consistent with the pseudo-second-order models.

Author Contributions: H.Q.; writing—original draft preparation, J.D.; writing—review and editing, D.P.; investigation; T.W.; investigation; H.Z.; investigation; R.P.; supervision. All authors have read and agreed to the published version of the manuscript.

Funding: This research received no external funding.

Conflicts of Interest: The authors declare no conflict of interest.

References

1. Sunil, K.; Karunakaran, G.; Yadav, S.; Padaki, M.; Zadorozhnyy, V.; Pai, R.K. Al-Ti₂O₆ a mixed metal oxide based composite membrane: A unique membrane for removal of heavy metals. *Chem. Eng. J.* **2018**, *348*, 678–684. [[CrossRef](#)]
2. Xu, L.; Wang, T.; Wang, J.; Lu, A. Occurrence, speciation and transportation of heavy metals in 9 coastal rivers from watershed of Laizhou Bay, China. *Chemosphere* **2017**, *173*, e61–e68. [[CrossRef](#)] [[PubMed](#)]
3. Xu, Y.; Zhang, C.; Zhao, M.; Rong, H.; Zhang, K.; Chen, Q. Comparison of bioleaching and electrokinetic remediation processes for removal of heavy metals from wastewater treatment sludge. *Chemosphere* **2017**, *168*, e1152–e1157. [[CrossRef](#)]
4. Sountharajah, D.P.; Loganathan, P.; Kandasamy, J.; Vigneswaran, S. Removing heavy metals using permeable pavement system with a titanate nano-fibrous adsorbent column as a post treatment. *Chemosphere* **2017**, *168*, e467–e473. [[CrossRef](#)] [[PubMed](#)]
5. Tag El-Din, A.F.; El-Khouly, M.E.; Elshehy, E.A.; Atia, A.A.; El-Said, W.A. Cellulose acetate assisted synthesis of worm-shaped mesopores of MgP ionexchanger for cesium ions removal from seawater. *Microporous Mesoporous Mater.* **2018**, *265*, 211–218. [[CrossRef](#)]
6. Barakat, M.A. New trends in removing heavy metals from industrial wastewater. *Arab. J. Chem.* **2011**, *4*, 361–377. [[CrossRef](#)]
7. Nguyen, T.A.H.; Ngo, H.H.; Guo, W.S.; Zhang, J.; Liang, S.; Yue, Q.Y.; Li, Q.; Nguyen, T.V. Applicability of agricultural waste and byproducts for adsorptive removal of heavy metals from wastewater. *Bioresour. Technol.* **2013**, *148*, 574–585. [[CrossRef](#)]
8. Xu, J.; Cao, Z.; Zhang, Y.L.; Yuan, Z.L.; Lou, Z.M.; Xu, X.H.; Wang, X.K. A review of functionalized carbon nanotubes and graphene for heavy metal adsorption from water: Preparation, application, and mechanism. *Chemosphere* **2018**, *195*, 351–364. [[CrossRef](#)]
9. Sarma, G.K.; Sen Gupta, S.; Bhattacharyya, K.G. Nanomaterials as versatile adsorbents for heavy metal ions in water: A review. *Environ. Sci. Pollut. Res.* **2019**, *26*, 6245–6278. [[CrossRef](#)]
10. Yao, H.; Zhang, X.F.; Hu, Z.H. The advantages of Shanglu biochar for Pb ion adsorption. *J. Shihezi Univ. (Nat. Sci.)* **2021**, *39*, 668–673.
11. Zhai, F.J.; Zhang, C.; Song, G.F.; Jiang, S.X.; Shan, B.Q.; Song, Z.X. The adsorption mechanism of kapok biochar on Cr(VI) in aqueous solution. *Acta Sci. Circumstantiae* **2021**, *41*, 1891–1900.
12. Wei, Z.P.; Zhu, Y.L.; Zhao, C.T.; Tang, J.X.; Gao, Y.X.; Li, M.X. Research Advances on Biochar Adsorption Mechanism for Heavy Metals and its Application Technology. *Chin. J. Soil Sci.* **2020**, *51*, 741–747.
13. Peng, R.C.; Li, H.; Chen, Y.T.; Ren, F.P.; Tian, F.Y.; Gu, Y.W.; Zhang, H.L.; Huang, X.R. Highly efficient and selectivity removal of heavy metal ions using single-layer Na_xK_yMnO₂ nanosheet: A combination of experimental and theoretical study. *Chemosphere* **2021**, *275*, 130068. [[CrossRef](#)]
14. Song, Y.Q.; Tan, Q.; Lin, B.Y.; Liao, L.; Zeng, C.; He, Z.Z.; Lin, B.Y.; Qiu, W.M. Controllable synthesis of MnO₂ with different crystal structures and their adsorption activity for heavy metals. *Inorg. Chem. Ind.* **2018**, *50*, 40–42, 53.
15. Peng, Q.; Guo, J.X.; Zhang, Q.R.; Xiang, J.Y.; Liu, B.Z.; Zhou, A.G.; Liu, R.P.; Tian, Y.J. Unique Lead Adsorption Behavior of Activated Hydroxyl Group in Two-Dimensional Titanium Carbide. *J. Am. Chem. Soc.* **2014**, *136*, 4113–4116. [[CrossRef](#)]
16. Ma, C.X.; Huangfu, X.L.; Ma, J.; Huang, R.X.; He, Q.; Liu, C.H.; Zhou, J.; Jiang, J.; Zhu, Y.Y.; Huang, M.H. Deposition Kinetics of Nanosized Manganese Dioxide in Presence of Divalent Cations. *China Water Wastewater* **2018**, *34*, 31–35.
17. Kim, E.J.; Lee, C.S.; Chang, Y.Y.; Chang, Y.S. Hierarchically Structured Manganese Oxide-Coated Magnetic Nanocomposites for the Efficient Removal of Heavy Metal Ions from Aqueous Systems. *ACS Appl. Mater. Interfaces* **2013**, *5*, 9628–9634. [[CrossRef](#)] [[PubMed](#)]
18. Zhang, W.J.; Kou, M. Applications of two dimensional material MXene in water treatment. *J. Mater. Eng.* **2021**, *49*, 14–26.
19. Hou, J.H.; Yang, M.Y.; Sun, A.; Cao, C.B. Application of MXenes and their composite materials in the field of environment. *Fine. Chemicals.* **2021**, *38*, 2422–2431.
20. Fan, M.; Wang, L.; Zhang, Y.J.; Pei, C.; Chai, Z.; Shi, W. Research progress of MXene materials in radioactive element and heavy metal ion sequestration. *Sci. Sin. Chim.* **2019**, *49*, 27–38. [[CrossRef](#)]
21. Leng, Y.Y.; Zhang, S.Y.; Zong, X.X.; Li, Y.F. Research Progress on New Low Dimensional Materials MXene. *Chem. Adhes.* **2016**, *38*, 450–454.
22. Wan, H.; Nan, L.; Geng, H.; Zhang, W.; Shi, H. Green Synthesis of A Novel MXene–CS Composite Applied in Treatment of Cr(VI) Contaminated Aqueous Solution. *Processes* **2021**, *9*, 524. [[CrossRef](#)]
23. Liu, Z.; Xu, K.; Sun, H.; Yin, S. One-Step Synthesis of Single-Layer MnO₂ Nanosheets with Multi-Role Sodium Dodecyl Sulfate for High-Performance Pseudocapacitors. *Small* **2015**, *11*, 2182–2191. [[CrossRef](#)]
24. Chen, S.; Xiang, Y.; Xu, W.; Peng, C. A novel MnO₂/MXene composite prepared by electrostatic self-assembly and its use as an electrode for enhanced supercapacitive performance. *Inorg. Chem. Front.* **2019**, *6*, 199–208. [[CrossRef](#)]
25. Dinh, V.P.; Le, N.C.; Nguyen, T.P.; Nguyen, N.T. Synthesis of α -MnO₂ Nanomaterial from a Precursor γ -MnO₂: Characterization and Comparative Adsorption of Pb(II) and Fe(III). *J. Chem.* **2016**, *2016*, 8285717. [[CrossRef](#)]
26. Zhao, Q.N.; Li, X.L.; Zhu, J.F.; Jiao, H.Y.; Huang, J.X. Manganese Dioxide Morphology on Electrochemical Performance of Ti₃C₂T_x@MnO₂ Composites. *J. Inorg. Mater.* **2020**, *35*, 119–125. [[CrossRef](#)]
27. Ren, Y.; Yan, N.; Feng, J.; Ma, J.; Wen, Q.; Li, N.; Dong, Q. Adsorption mechanism of copper and lead ions onto graphene nanosheet/ δ -MnO₂. *Mater. Chem. Phys.* **2012**, *136*, 538–544. [[CrossRef](#)]
28. Lin, M.; Chen, Z. A facile one-step synthesized epsilon-MnO₂ nanoflowers for effective removal of lead ions from wastewater. *Chemosphere* **2020**, *250*, 126329. [[CrossRef](#)]

29. Guo, J.; Chen, T.; Zhou, X.; Zheng, T.; Xia, W.; Zhong, C.; Liu, Y. Preparation and Pb (II) adsorption in aqueous of 2D/2D g-C₃N₄/MnO₂ composite. *Appl. Organomet. Chem.* **2019**, *33*, e5119. [[CrossRef](#)]
30. Xia, W.; Liu, Y. Preparation of MnO₂ modified magnetic graphitic carbon nitride composite and its adsorption toward Pb(II) in waste water. *Water Pract. Technol.* **2021**, *16*, 1498–1509. [[CrossRef](#)]